

Solid-State Deuterium NMR Studies of Organic Molecules in the Tectosilicate Nonasil

Daniel F. Shantz and Raul F. Lobo*

Center for Catalytic Science and Technology, Department of Chemical Engineering, University of Delaware, Newark, Delaware 19716

Received: September 29, 1997; In Final Form: January 14, 1998

Solid-state deuterium NMR spectroscopy is used to study the dynamics of organic molecules occluded in the as-synthesized high-silica tectosilicate nonasil. The nonasil samples are synthesized using trimethylalkylammonium structure-directing agents to determine the role of electrostatic interactions. Size effects are quantified by performing ^2H NMR spin–lattice (T_1) relaxation experiments, and the mobility of the substituent alkyl groups is studied using ^2H MAS NMR. The charge-compensating defect sites are characterized using ^{29}Si and ^1H NMR. The motion of the trimethylammonium group of the structure-directing agent is a composite motion of methyl group rotations and rotation about the nitrogen C_3 axis in all samples down to 190 K. The ^2H T_1 and ^2H MAS NMR results illustrate the steric confinement the nonasil cage exerts on the larger ($C_n \geq C_5$) substituent alkyl groups. Isotropic motion is not observed for any of the structure-directing agents at 370 K, indicating strong organic–inorganic interactions. This is in sharp contrast to nonasil samples made with electrically neutral amines where rapid isotropic reorientation is observed at room temperature. These results have interesting implications in zeolite synthesis. For aluminosilicates synthesized with charged structure-directing agents, similar organic–inorganic interactions may allow for aluminum preferentially occupying specific framework sites. This could lead to tailoring the distribution of catalytic sites in zeolites based on the charge distribution of the structure-directing agent.

Introduction

Electrostatic forces play a fundamental role in many physical and chemical systems, including protein structure and stability, ionic conduction, the properties of many colloidal systems, self-assembly, etc.¹ The important role of electrostatic forces in the determination of the catalytic, adsorptive, and other properties of zeolites and other microporous systems has long been recognized.² Zeolites are crystalline microporous materials used industrially as heterogeneous catalysts and as adsorbents in gas separations and purifications.³ The motion of organic molecules in zeolites is complex because the pores of a zeolite are nearly the same size as the organic molecules occluded in them.⁴ The mobility of an organic molecule is largely determined by the forces between an organic molecule and the zeolite framework, and strongly influences macroscopic properties such as the diffusivity and catalytic activity. These interactions have received considerable attention in recent years and remain a subject of active research.⁵

Synthetic high-silica zeolites are prepared using an organic molecule, usually a quaternary ammonium cation, in the synthesis mixture. The organic molecule is often called a structure-directing agent (SDA) because the shape and size of the molecule strongly influence the structure of the final synthesis product. Usually a close relationship is observed between the size and shape of the organic molecule, and the size and shape of the zeolite pores and pore intersections.⁶ ZSM-5, ZSM-18, and SSZ-26 are three examples where the zeolite structure clearly reflects the geometry and size of the structure-

directing agent.^{7–9} It is also believed that electrostatic interactions play an important role in this molecular recognition process.

Before a high-silica zeolite can be used in catalytic, adsorption, or ion-exchange applications, the structure-directing agent needs to be removed by heating at high temperatures in the presence of oxygen (calcination). There is an extensive body of work on the characterization of zeolites and related materials (after calcination) using diffraction, microscopy, and spectroscopic techniques.¹⁰ On the other hand, relatively little characterization work has been done of the organic–inorganic composite material obtained directly from synthesis. The objective of this work is to investigate as-made zeolites and to characterize the interactions between the organic and inorganic components. Electrostatic interactions are of particular interest as they are not well understood, yet have important implications in not only the physical properties of zeolites, but also in the synthesis of zeolites and the process of structure-direction.

The tectosilicate nonasil (NON), originally synthesized by Marler et al.,¹¹ is used as a model system for this work. Nonasil is a clathrasil, a class of natural and synthetic materials with cages, in contrast to zeolites which have one- or multidimensional open pore structures. The framework of nonasil can be constructed from 9-hedra bounded by one four-membered ring and eight five-membered rings [4^15^8 unit]. The nonasil material has three cages formed by (1) the 4^15^8 unit, (2) an 8-hedra formed by four five-membered rings and four six-membered rings [5^46^4 unit], and (3) a 20-hedra formed by eight five-membered rings and twelve six-membered rings [5^86^{12} unit]. The three cages have free volumes of approximately 30, 25, and 290 Å³, respectively, and the organic structure-directing agents are only found in the largest cage [5^86^{12}].¹¹ There are four 5^86^{12} cages per unit cell (see Figure 1) and the free

* Corresponding author: Center for Catalytic Science and Technology, Department of Chemical Engineering, University of Delaware, Newark, DE. Phone: (302) 831-1261. Fax: (302) 831-2085. E-mail: lobo@che.Udel.edu.

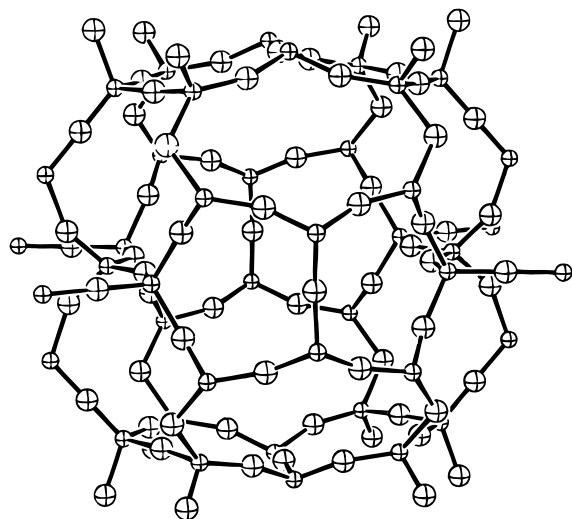


Figure 1. Large $[5^86^{12}]$ cage of nonasil.

dimensions of the large cage are approximately $9.8 \times 11.6 \times 9.8$ Å. Marler et al.¹¹ determined the structure using single-crystal X-ray diffraction refining the structure in the orthorhombic space group $Fmmm$ with unit cell lattice constants $a_0 = 22.232$ Å, $b_0 = 15.058$ Å, and $c_0 = 13.627$ Å. The space group $Fmmm$ is the highest topological symmetry for the NON topology. Gies and Marler used electrically neutral molecules such as 2-methylpyrrolidine, 2-aminopentane, and 2-methylpiperidine to synthesize the nonasil samples and found that the structure-directing agents were positionally disordered in the as-made material. If boron is present in the synthesis mixture, nonasil crystallizes in the orthorhombic space group $Cmca$.¹²

Harris and Zones¹³ synthesized nonasil using several trimethylalkylammonium compounds as structure-directing agents and performed energy minimizations using molecular mechanics calculations. Balkus and Shepelev¹⁴ have synthesized nonasil using bis(cyclopentadienyl)cobalt(III) hydroxide ($[\text{Cp}_2\text{Co}]^+\text{OH}^-$), and Behrens et al.¹⁵ synthesized nonasil with $[\text{Cp}_2\text{Co}]^+$ but prepared by the fluoride method.¹⁴ The structure of fluoride $\text{Cp}_2\text{Co(III)-NON}$ was refined in the orthorhombic space group $Pccn$.¹⁶ Their single-crystal X-ray work shows that the metallocene complex is ordered in the nonasil cage and forms hydrogen bonds between the Cp hydrogens and the oxygen atoms in the nonasil framework. In contrast, Gies¹⁷ has shown that electrically neutral amines used to synthesize nonasil isotropically reorient on the microsecond time scale.

Solid-state NMR is a powerful tool for probing the local structure of zeolites^{10d,18} and solid materials in general.^{18,19} ²⁹Si and ²⁷Al NMR are useful to investigate the local structure of the framework atoms,^{10d,20} and ²³Na, ⁷Li, and ¹³³Cs NMR compliment diffraction techniques for characterizing the location, site populations, and mobility of extraframework cations in zeolites.²¹ ²H NMR can be used to obtain detailed information about the dynamics of organic molecules occluded inside the zeolite micropores.²² Deuterium has a nuclear spin $I = 1$, a static quadrupole coupling constant between 150 and 200 kHz, and it is an experimentally convenient quadrupolar nuclei because the quadrupolar interaction dominates dipole–dipole coupling and chemical shift effects. Another advantage is that the quadrupole interaction is small enough that the whole powder spectrum can be observed with high-power pulsed NMR methods.²³ The main limitation of ²H NMR spectroscopy is that it requires the use of isotopically enriched samples. The value of the quadrupole coupling constant (QCC), an experimentally measurable quantity, is determined by the rate and

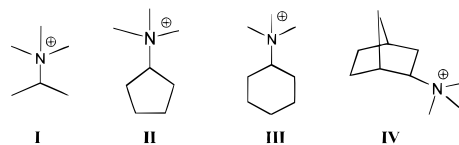


Figure 2. Organic molecules used as structure-directing agents for the synthesis of nonasil.

geometry of molecular motion.²³ Rotations that are fast on the ²H NMR time scale result in a narrowing of the signal (Pake doublet) as compared to the static value of approximately 120 kHz. For motion with axial symmetry (i.e., $\eta = 0$) (the asymmetry parameter η is defined as $\eta = (V_{xx} - V_{yy})/V_{zz}$, where V_{xx} , V_{yy} , and V_{zz} are the diagonal elements of the electric field gradient (EFG) tensor, and for motions with a 3-fold or higher axis of symmetry, typically $\eta = 0$),²⁴ the frequencies of the horns of the Pake doublet are determined by

$$\nu = \pm \sqrt[3]{\frac{2\pi e^2 q Q}{h}} (3 \cos^2 \theta - 1)$$

where $(2\pi e^2 q Q/h)$ is the static quadrupole coupling constant ($\sim 2\pi \times 170$ kHz), h is Planck's constant, Q is the nuclear quadrupole moment, $eq = V_{zz}$ is the principal component of the EFG tensor, and θ is the angle between the rotation axis and the magnetic field in the laboratory frame. Motions that are fast on the ²H NMR time scale can be quantified using spin–lattice (T_1) relaxation experiments in conjunction with NMR line shape simulations.^{24–26} Several groups have used ²H NMR to study the interactions between aromatic molecules and extraframework cations in faujasite-type zeolites.²⁷ These studies showed a strong interaction between the extraframework cations and the π -system of the aromatic molecule (i.e., energies of activation of ~ 25 kJ/mol were observed). ²H NMR has been used extensively to study the dynamics of organics in inclusion compounds,²⁸ although little work has been done with as-synthesized zeolites.²⁹

This work investigates the dynamics of charged structure-directing agents occluded inside the large $[5^86^{12}]$ cage of nonasil (Figure 1). Electrically neutral amines used to synthesize nonasil and other clathrasils isotropically reorient and exhibit only weak interactions between the organic molecules and the zeolite framework.¹⁷ The results for the electrically neutral amines are similar to many ²H NMR studies of organic molecules in inclusion compounds where steric constraints and van der Waals interactions dominate molecular motion.²⁸ In contrast, we are employing cationic structure-directing agents in the synthesis of nonasil and our results should point out the effects of electrostatic forces. There are four advantages to using nonasil as a model system: (1) interactions between structure-directing agents are negligible, (2) nonasil is an all-silica material³⁰ so there are no extraframework cations, (3) the same phase can be prepared with organic molecules of different size, and (4) since the structure of nonasil is related to the structure of other high-silica zeolites, our results can be qualitatively extended to other microporous silicates.

Samples of nonasil synthesized with molecules **I–IV** (see Figure 2) have been characterized using X-ray diffraction (XRD), scanning electron microscopy (SEM), and nuclear magnetic resonance spectroscopy (NMR). Solid-state deuterium NMR is used to study the dynamics of the organic molecules occluded in the nonasil samples. Different parts of the organic molecules are selectively labeled with deuterium. Our results

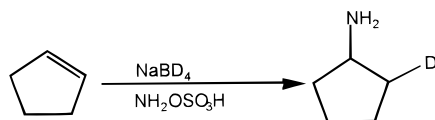
indicate that, for all structure-directing agents used, the trimethylammonium segment of the molecule is rapidly rotating along the R–N and N–C bonds and that the large substituent alkyl groups ($C_n \geq C_5$) are nearly immobile in the nonasil cage. The lack of isotropic reorientation in all samples up to 370 K indicates that electrostatic forces between the framework and the structure-directing agent prevent the molecule from isotropic motion, in contrast to nonasil made with electrically neutral amines.¹⁷

Experimental Section

Sample Preparation. Nonasil samples are synthesized using a modification of the method reported by Harris and Zones¹³ with the four trimethylalkylammonium compounds **I–IV** (Figure 2) as structure-directing agents. The four structure-directing agents used are *N,N,N*-trimethylisopropylammonium (TMC3), *N,N,N*-trimethylcyclopentylammonium (TMC5), *N,N,N*-trimethylcyclohexylammonium (TMC6), and *N,N,N*-trimethylnorbornylammonium (TMC7).

Synthesis of *N,N,N*-trimethylcyclopentylammonium Iodide. TMC5 is prepared by adding 100 mmol of cyclopentylamine (99% Aldrich) and 20 g of anhydrous K_2CO_3 (85+% Fisher) to 100 mL of methanol (99% ACS reagent, Fisher). The amine is alkylated with 50% excess methyl iodide (99% Aldrich), and the solution is allowed to react for 24 h in the absence of light at room temperature. The liquid phase is separated from the solids by filtration. Solvent and other volatile components are removed under vacuum at 50–60 °C using a rotavapor yielding the crude TMC5 salt (~85% yield) as a white powder. The crude template is recrystallized from a boiling 70:30 ethyl acetate/methanol mixture (V/V) which is cooled to 5 °C and left overnight (~40% yield). Three grams of the recrystallized TMC5 salt are ion-exchanged to the hydroxide form using a 5-fold excess of resin (IONAC NA-38, OH^- form) for 24 h. The conversion of the iodide to hydroxide is greater than 95% based on titration of the resultant solution. The other structure-directing agents can be made using the same procedure with similar yields. The ^{13}C NMR results for the recrystallized iodide salts in D_2O are TMC3–iodide $\delta = 67.5, 51.2, 17.1, 15.1$ ppm; TMC5–iodide $\delta = 71.2, 51.9, 28.0, 24.2$ ppm; TMC6–iodide $\delta = 74.4, 51.6, 26.6, 24.9, 24.5$ ppm; TMC7–iodide $\delta = 78.9, 51.8, 37.8, 37.0, 36.1, 34.7, 28.9, 26.4$ ppm.

Preparation of Deuterium-Labeled Structure-Directing Agents. Synthesis of structure-directing agents selectively labeled with deuterium in the methyl groups is carried out as described above except d_3 - CD_3I (99%+d Aldrich) is used instead of CH_3I in the alkylation step. A procedure described by Brown et al.³¹ is used to synthesize ring-deuterated primary amines (**II–IV**) with deuterium β to the amine group. The overall reaction is



Synthesis of d_1 -Cyclopentylamine. A flame-dried 250 mL round-bottom flask is fitted with a dried condenser and dropping funnel and purged using dry argon. 60 mL of diglyme (99%, Fisher) are added to the flask and 2 g of $NaBD_4$ (99%-d, Aldrich) are added to the diglyme. After 15 min of mixing, 10.2 mL of cyclopentene (99+%, Aldrich) are added via a syringe. The flask is then set in an ice bath and 8.1 mL of BF_3OEt_2 (99%, Aldrich) are added to the dropping funnel using

TABLE 1: Nonasil Synthesis Conditions

sample ^a	molar ratios in the synthesis gel	synthesis temperature, K
TMC3–NON	1 SiO_2 :0.15 R^+OH^- :0.125 NaOH:45 H_2O	433
TMC5–NON	1 SiO_2 :0.15 R^+OH^- :0.10 NaOH:45 H_2O	433
TMC6–NON	1 SiO_2 :0.15 R^+OH^- :0.125 NaOH:45 H_2O	443
TMC7–NON	1 SiO_2 :0.15 R^+OH^- :0.15 NaOH:45 H_2O	433

^a TMC3 (**I**): *N,N,N*-trimethylisopropylammonium hydroxide. TMC5 (**II**): *N,N,N*-trimethylcyclopentylammonium hydroxide. TMC6 (**III**): *N,N,N*-trimethylcyclohexylammonium hydroxide. TMC7 (**IV**): *N,N,N*-trimethylnorbornylammonium hydroxide.

a syringe. The BF_3OEt_2 is added dropwise to the flask while immersed in the ice bath. The mixture is allowed to react for 3 h, after which 14.4 g of hydroxylamine-*o*-sulfonic acid (99%, Aldrich) dissolved in 50 mL diglyme are added to the mixture dropwise. The mixture is heated to 100 °C and allowed to react for 3 h. The resulting solution is cooled and made acidic (pH < 2) with concentrated HCl. The resultant mixture is extracted three times with ether to remove any residual boric acid, and the organic phase is discarded. The aqueous phase is made strongly basic (pH > 12) using NaOH and is again extracted three times with ether. The ether is removed at reduced pressure, and the crude solid recovered is alkylated as described previously. The yield from the reaction is approximately 50%. The selective deuterium-labeling of the rings was verified by ^{13}C solution NMR (see Supporting Information).

Nonasil Synthesis. The nonasil synthesis gel stoichiometry varies slightly depending on the structure-directing agent used (see Table 1). The synthesis gel molar ratios are 1 SiO_2 :0.15 R^+OH^- :0.125 NaOH:45 H_2O , where R^+OH^- is the structure-directing agent exchanged to the hydroxide form. The main difference in the synthesis conditions is the adjustment of the amount of sodium.

For example, the TMC5–nonasil sample is prepared by mixing 2.4 g of Cab-O-Sil (M5 grade), 20 mL of 0.3 N *N,N,N*-trimethylcyclopentylammonium hydroxide, and 13.4 mL of deionized water. After a homogeneous mixture is obtained, 0.16 g of NaOH (pellets 95+%, Aldrich) are ground into a fine powder and added to the solution. The solution is mixed for approximately 1 h, until a liquidlike gel is obtained. The solution is sealed in two 23 mL Teflon-lined Parr autoclaves which are heated at 160 °C for 7 days under autogenous pressure and rotated at 30 rpm. The autoclaves are cooled to room temperature after the synthesis period. The solids are collected by filtration, washed several times with deionized water, and dried overnight at 80 °C. Seeding was used only for the synthesis of TMC3–NON which was seeded with 1 wt % TMC5–NON crystals. None of the samples used in the deuterium NMR studies were seeded.

Samples are also prepared using D_2O (99.9%-d, Aldrich) as the solvent. For these samples, ion-exchange, titration of the exchanged structure-directing agent, and the nonasil synthesis mixture preparation are performed in a glovebag under a dry argon atmosphere.

Analytical. Powder X-ray diffraction (XRD) is performed on samples using a Phillips 3000 X'Pert System with $Cu K\alpha$ radiation. The patterns used for indexing are collected from 4°–50° 2θ using the step scan mode, a 0.02° step size, and 15 s count time per step. The peak deconvolution was carried out using the Phillips package ProFit and refinement of the unit

cell parameters was done using the program Lapod.³² Scanning electron microscopy was done using a JEOL 850 at 10 kV. Solution ¹³C NMR spectra were measured on a Bruker AC 250 spectrometer at 62.26 MHz with the chemical shifts referenced to tetramethylsilane. ²⁹Si, ¹³C, ¹H, and ²H solid-state NMR spectra were measured on a Bruker MSL 300 spectrometer at 59.63, 75.47, 300.13, and 46.07 MHz, respectively. The chemical shifts for the ²⁹Si, ¹³C, and ¹H spectra were referenced to tetramethylsilane. The ²⁹Si MAS NMR spectra were acquired using a 7 mm probe with ZrO₂ rotors, a spin rate of 3 kHz, and a 100 s recycle delay to avoid relaxation effects in the signal intensities. The structural integrity of the structure-directing agents inside the as-made nonasil samples was verified by ¹³C CP-MAS NMR using a contact time of 5 ms, a spin rate of 3 kHz, a 90° ¹H pulse of 6 μs, and high-power proton decoupling. ¹H MAS spectra were acquired using a 4 mm probe with ZrO₂ rotors, a spin rate of 9 kHz, a 30 s recycle delay, and a 4 μs 60° pulse.

The static ²H NMR experiments were performed using the usual quadrupole echo pulse sequence³³ with a 90° pulse of 3.25 μs unless otherwise noted, a pulse spacing of 30 μs, and recycle delays between 1 and 3 s. Variable pulse spacing experiments were performed at room temperature to check for distortions in the quadrupole echo.³⁴ Variable-temperature experiments were performed from the low to the high-temperature range of the probe (190 to 370 K). The temperature was controlled with a Bruker B-1000 temperature controller to within ±1K with an accuracy of ±2K. Temperature calibration for the probe was done by placing a thermocouple inside the sample chamber and comparing the results to a calibrated thermocouple located inside the probe, just outside the sample chamber, over the temperature range of 190–370 K. Spin–lattice (*T*₁) relaxation experiments were performed using a 6.5 μs 180° pulse and the phase cycling suggested by Vold.²⁵ ²H magic-angle spinning (MAS) NMR, as described by Jakobsen et al.,³⁵ was used for the analysis of samples selectively labeled with deuterium on the rings β to the trimethylammonium group due to signal-to-noise improvements. The ²H single-pulse MAS NMR spectra were obtained using a 4 mm MAS probe, a 45° pulse of 4 μs, a recycle delay of 4 s, and a spin rate (*ν*_r) of 6 kHz, unless noted. ²⁹Si NMR line shape simulations and ²H NMR line shape fitting were done using software written in-house. ²H NMR line shape simulations using different motion models were done using TurboPowder and FastPowder.²⁶

Elemental analysis for H, C, N, Si, and Na was done by Galbraith Laboratories (Knoxville, TN) and Chevron R & D (Richmond, CA). Molecular dynamics simulations and energy minimizations were performed using the Biosym-MSI package Cerius 3.2. The Burchart-Universal force field was used in all simulations. The molecular dynamics simulations were ran for a 10 ns long trajectory with a 0.01 ps time step at 300 K, using the NVT ensemble and a Nosé thermostat. All simulations used a rigid, defect-free framework, and the initial conformation of the structure-directing agent used was found using the energy minimization routine.

Results and Discussion

Material Characterization. The X-ray diffraction patterns for the nonasil samples prepared with molecules **I**, **II**, **III**, and **IV** are shown in Figure 3. The as-made materials are highly crystalline nonasil, no impurities or diffuse scattering background are detected by either XRD or SEM. Scanning electron micrographs (see Supporting Information) indicate that most of the crystallites are greater than 1 μm in size. The micrographs

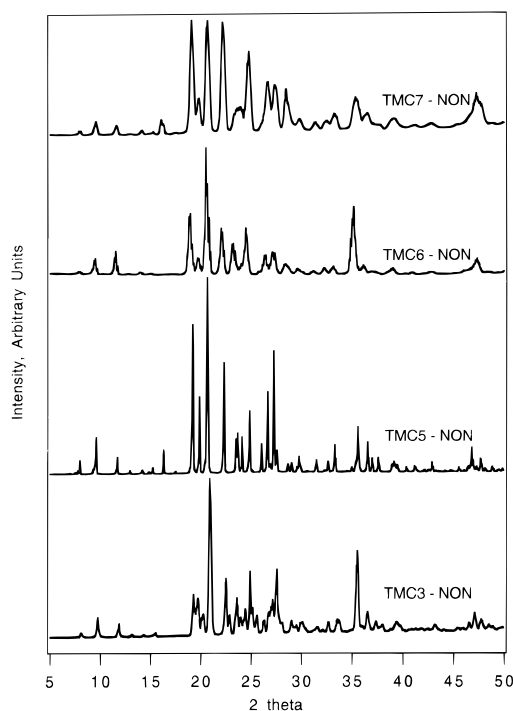


Figure 3. X-ray powder diffraction patterns of nonasil samples.

TABLE 2: Unit Cell Lattice Constants for Nonasil Samples

structure-directing agent	<i>a</i> (Å)	<i>B</i> (Å)	<i>c</i> (Å)	α	β	γ
TMC3–NON	22.08	15.03	13.74	90.7°	90.1°	90.2°
TMC5–NON	22.15	15.14	13.69	90°	90°	90°
TMC6–NON	23.26	15.04	13.55	90.71°	90.11°	90.17°
TMC7–NON	22.00	15.27	13.67	90°	90°	90°
2-aminopentane ¹¹	22.23	15.05	13.62	90°	90°	90°

for all samples show a nearly spherical morphology. The crystal size depends on which structure-directing agent is used, but in all samples, smaller crystals (~1 μm) with the same morphology are observed on the surface of the larger crystals. The TMC5 structure-directing agent forms the largest crystals (30–40 μm), and the TMC3 structure-directing agent forms the smallest crystals (1–8 μm). As it can be observed in the XRD patterns (Figure 3) some of the samples show very sharp peaks (TMC5–NON) while others show broad peaks (TMC3–NON). These differences are not due to crystal size effects as the crystals in all cases are larger than 1 μm. Inspection of the TMC6–NON XRD pattern shows the splitting of the 111 reflection into 4 distinct peaks, (111, $\bar{1}\bar{1}\bar{1}$, $\bar{1}\bar{1}1$, and $1\bar{1}\bar{1}$) suggesting that the actual symmetry of the material is triclinic and not orthorhombic. For this reason the TMC3–NON and TMC6–NON samples have been indexed using a triclinic unit cell. The TMC7–NON is also of lower symmetry, but due to extensive peak overlap, it has been indexed using a pseudo-orthorhombic unit cell. Note that due to the strong peak overlap the unit cell parameters of TMC3–NON and TMC7–NON are only approximate. The refined unit cell lattice constants for the samples are tabulated in Table 2 and are in good agreement with previously reported values.¹¹ The changes in symmetry are not surprising, as several zeolitic systems exhibit changes in symmetry either due to a change of temperature or the presence of adsorbates.^{10a} As noted in the Introduction, the symmetry of nonasil samples depends heavily on the structure-directing agent.

Nonasil has not been successfully synthesized in the absence of a structure-directing agent. The large [5⁸6¹²] cage of nonasil must be occupied by a molecule to help stabilize the structure.

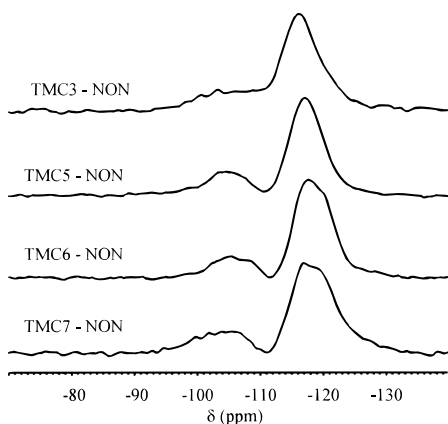


Figure 4. ^{29}Si MAS NMR spectra of as-made nonasil samples.

TABLE 3: Summary of ^{29}Si MAS NMR Spectra Simulations

structure-directing agent	Q^3		Q^4		Q^3/Q^4	no. of Q^3 per cage
	chemical shift, δ (ppm)	relative intensity, I	chemical shift, δ (ppm)	relative intensity, I		
TMC3	-102.7	15.6	-116.3	81.6	0.23	4.1
	-107.7	2.8				
TMC5	-104.6	18.6	-117.3	81.4	0.23	4.1
	-108.6	2.1	-120.3	47.2		
TMC6	-104.7	14.9	-116.9	35.8	0.20	3.7
	-102.4	13.6	-116.4	26.1		
TMC7	-102.4	13.6	-116.4	26.1	0.22	4.0
	-106.6	4.5	-119.9	55.8		

The large cage could be occupied by the structure-directing agent, byproducts of structure-directing agent degradation, or sodium. The ^{13}C CP-MAS spectra unambiguously confirm that the structure-directing agents are all intact inside the nonasil cages (see Supporting Information). The elemental analyses indicate that at least 80–90% of the cages are occupied by an organic structure-directing agent.³⁶ There is also less than 1 wt % sodium in the as-made materials. The small amount of sodium present is consistent with previous results for as-made high-silica zeolites, where also a small amount of Na^+ was found occluded in the final product.^{5c}

The ^{29}Si MAS NMR spectra of the as-made materials are shown in Figure 4. We have found that consistent with previous reports,³⁷ nonasil samples prepared using cationic structure-directing agents contain a large number of silanol groups. Each spectrum contains two broad lines, one line is in agreement with silicon atoms adjacent to one siloxy or silanol group (Q^3 , where Q^n stands for $\text{X}_{4-n}\text{Si}[\text{OSi}]_n$, $\text{X} = \text{OH}$ or O^-)^{10d} and the second line is consistent with silicon atoms bonded to four silicon atoms via an oxygen atom (Q^4). Note that contributions to the Q^3 intensity from surface silanols are negligible due to the crystal sizes; we have calculated that less than 0.2% of the silicon atoms would be surface silanol groups for a defect-free $5 \times 5 \times 5 \mu\text{m}$ crystal. This results in a Q^3/Q^4 of 2×10^{-5} .

The ratio of integrated intensity of the Q^3/Q^4 lines is directly related to the number of silanol groups in the as-made material (see Table 3). Most all-silica zeolites are made with cationic structure-directing agents and charge neutrality requirements result in the formation of a charge-compensating defect site.³⁸ The quantity and nature of these defects, which can strongly affect the physical properties of zeolites, are as yet unclear.³⁹ Koller et al.³⁷ have shown that a siloxy group is the charge compensator for the cationic structure-directing agent and not the hydroxide anion. Lobo et al.^{6d} have observed that the number of defects in the as-made nonasil material is much larger

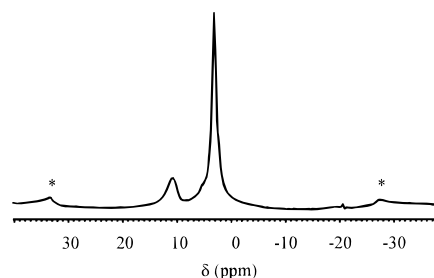


Figure 5. ^1H NMR spectrum of TMC5–NON. (Asterisks denote spinning sidebands).

for samples made with cationic structure-directing agents than samples made with neutral amines. Moreover, additional silanol groups are present in excess of the siloxy and silanol groups needed to balance the cationic charge on the structure-directing agent. The integrated intensities of the spectra result in Q^3/Q^4 values of 0.23, 0.23, 0.20, and 0.22 for the TMC3–NON, TMC5–NON, TMC6–NON, and TMC7–NON samples, respectively, corresponding to approximately four Q^3 sites per cage (there are 22 Si atoms per $[\text{S}^{86}\text{I}^{12}]$ cage). The results of fitting the spectra are given in Table 3. Note that number of lines used to fit each Q^n line (1 or 2) was chosen to minimize the error between the experimental and simulated line shapes (i.e., they do not represent crystallographically inequivalent sites). These results are in good agreement with the work of Koller et al.³⁷ which reports a $\text{Q}^3/\text{N}^+ \sim 4$ for several all-silica materials. Our nonasil samples have no Q^2 or Q^1 groups, so the structure-directing agents are confined to one cage. The structure-directing agents cannot move through the six-membered rings of the nonasil framework; they need larger apertures in order to move between cages. Only framework sites with more than one of their Si–O–Si bonds broken could facilitate intercage mobility.

To investigate the effect of the small amount of sodium (<1 wt %) occluded in all of the nonasil samples, we prepared a sample of TMC5–NON without sodium in the synthesis mixture. The Q^3/Q^4 value calculated from the ^{29}Si NMR spectrum of that sample also corresponds to four Q^3 per cage, therefore the sodium ions do not appreciably contribute to the quantity of defect sites in our samples.

The spatial proximity of the Q^3 groups cannot be determined from the ^{29}Si NMR results, however, this can be studied using ^1H NMR. The ^1H NMR spectrum of the TMC5–NON sample is shown in Figure 5. Two lines are present in the spectra for all the as-made materials, a broad line at 3 ppm assigned to the protons on the organic structure-directing agents and a line at 10.3 ppm. The broad line at 3 ppm is asymmetric and also has a shoulder at 4.5 ppm due to a small amount of water present in the sample. Koller et al.³⁷ observed a line at 10.2 ppm (± 0.2 ppm) for a series of as-made high-silica zeolites, including a nonasil sample made with the TMC7 structure-directing agent. Their work concluded that the line at 10.2 ppm was due to silanol groups engaged in hydrogen bonding with siloxy groups with an average Si–OH \cdots O–Si distance of ~ 2.6 Å. Using known chemical shift correlations⁴⁰ our results suggest an average OH \cdots O–Si distance of ~ 2.7 Å, in agreement with Koller et al.³⁷ within experimental error. The ^1H NMR spectra verify that some of the Q^3 sites in the framework are in close proximity, either as isolated pairs or in clusters.

Deuterium NMR. The deuterium NMR spectroscopy work consists of four parts. First, the ^2H NMR spectra of the neat solid salts with deuterium at the methyl groups are described. Second, ^2H NMR spectroscopy results of the nonasil samples

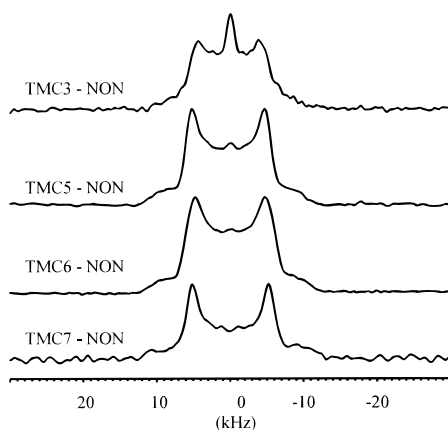


Figure 6. Static ^2H NMR spectra for d_9 -nonasil samples at 298 K.

made with structure-directing agents with labeled methyl groups are discussed. Third, we discuss ^2H spin–lattice (T_1) relaxation experiments done in conjunction with line shape simulations for the d_9 -labeled samples to complement the variable temperature experiments. Finally, the ^2H MAS NMR results for samples with labeled alkyl groups will be discussed. The characterization work has verified that the samples are all highly crystalline nonasil with the organic structure-directing agents intact inside the $[5^86^{12}]$ cage. These results do not however, imply long-range ordering of the structure-directing agents or the defect sites. Disorder of the defect sites or the structure-directing agents could result in molecules having a distribution of mobilities. Our results, however, seem to indicate that at least for the methyl groups the motion is uniform. All ^2H NMR line shape simulations were performed using the programs FastPowder and TurboPowder.²⁶

The motion of the structure-directing agents in the as-made nonasil samples can be well characterized using ^2H NMR. Recall that deuterons whose motions are slow on the ^2H NMR time scale ($\sim 10^{-7}$ s) result in a splitting between the horns of the Pake doublet of roughly 120 kHz. Rapid internal reorientation of the methyl groups but no rotations along the nitrogen C_3 axis reduces the splitting to ~ 40 kHz.¹⁹ Rapid rotations along both the nitrogen C_3 axis and the methyl group C_3 axes reduce the splitting to about 14 kHz (QCC = 18.8 kHz).^{22b} Also, since all of the above motions should be axially symmetric, the asymmetry parameter η should be zero.

^2H NMR Spectra of the Structure-Directing Agents in Nonasil. The ^2H NMR spectra of the d_9 -nonasil samples at 298 K are shown in Figure 6. Simulations of the d_9 -TMC5-, -TMC6, and -TMC7 nonasil spectra at 298 K yield QCCs of 15.1, 15.2, and 15.5 kHz and asymmetry values η of 0.05, 0.06, and 0.06, respectively. These values are similar to the neat solids (summarized in Table 4), with the exception of the TMC3 salt whose spectrum is a Lorentzian line with a full-width at half-maximum of 456 Hz (see Supporting Information). The simulated line shape of the d_9 -TMC3 nonasil sample yields a QCC of 13.5 kHz and an asymmetry value of 0.14, which are different from the other samples and are discussed in detail below. The motions of the occluded organics consist at least of fast rotations along both the nitrogen and methyl group C_3 axes. The values of the QCCs are lower than would be expected for only two rotations, even with the nonzero asymmetry.^{22b,41} The static quadrupole coupling constant could not be obtained for any of the samples because neither of the rotations were in the slow motion regime at 190 K; consequently, the following analysis will assume the static QCC is approximately 170 kHz.^{19,24,41}

TABLE 4: Quadrupole Coupling Constant, Asymmetry Parameter, and Spin–Lattice Relaxation Time (T_1) for d_9 -Labeled TMC7-, TMC6-, TMC5-, and TMC3–Nonasils, and Neat Salts at 298 K

sample	quadrupole coupling constant (kHz)	asymmetry parameter, η	T_1 (ms)
TMC7–NON	15.5	0.05	18.9
neat TMC7	$\sim 15.6^a$	N/A ^a	
TMC6–NON	15.2	0.06	21.7
neat TMC6	13.9	0.06	
TMC5–NON	15.1	0.05	24.7
neat TMC5	15.0	0.05	
TMC3–NON	13.5	0.14	45.2
neat TMC3	~ 0	N/A	

^a The motion of the TMC7 solid is in the intermediate motion regime so the QCC can only be estimated.

There are several possibilities that could explain the decrease in the QCC value (~ 15 kHz) from the expected value (~ 19 kHz) if only two rotations are present. One possible reason for this reduction in the averaged QCC could be the presence of additional motions. Specifically, the reduced QCC values can be accounted for by allowing an outward bending of the D–C–N bond angles on average of 4° . The breathing motion also introduces asymmetry into the line shape as the breathing motion has a pseudo 2-fold symmetry axis. The simulated NMR spectrum assuming an average bending of four degrees results in an averaged QCC of 15.1 kHz, consistent with the d_9 -TMC5 and d_9 -TMC6 nonasil results (see Supporting Information). The d_9 -TMC7 spectrum can be simulated accurately assuming a bending motion on average of 3° .

Another possible explanation of the observed reductions in the QCCs is the presence of librational motion. The decrease of the QCCs as the SDA gets smaller are in agreement with this conclusion. Clearly, for the TMC3–NON, the breathing motion is not sufficient to account for the obtained QCC. However, while the breathing motion is straightforward to simulate, the librational motion is not. The NMR results obtained cannot rule out one possibility over the other, and both could in fact be present. This is almost certainly the case for the TMC3–NON sample.

In addition to molecular motion, the reduction in the splitting of the Pake doublet could be due to large deviations from tetrahedral geometry in either the R–N–C bond angle, the N–C–D bond angle, or both. Distortions of the electric field gradient around the deuteron could also result in a lowering of the QCC value. Large deviations from tetrahedral geometry seem unlikely as both the methyl group rotations and the R–N bond rotation are fast on the NMR time scale. Distortions in the electric field gradient could be possible due to the cationic nature of the structure-directing agents, but would be very difficult to quantify. The case of a large nonzero asymmetry ($\eta = 0.2$) for an axially symmetric motion was recently reported by Griffin and co-workers on $[\text{W}(\text{Cp}^*\text{Me}_4)][\text{PF}_6]$.⁴² Their work suggests that deviations from tetrahedral geometry were primarily responsible for the observed asymmetry, and distortions of the electric field gradient (EFG) could be present, but were less significant. This conclusion was drawn based on the structure of the compound determined from crystallographic work.

If an additional motion is present, it is likely a breathing motion of the methyl groups, a librational motion of the SDA, or both. Either of the motions would also introduce asymmetry into the line shape which is observed for all samples. The nonzero asymmetry is unusual since motions that can be modeled as rotations about a 3-fold axis (i.e., fast rotation of

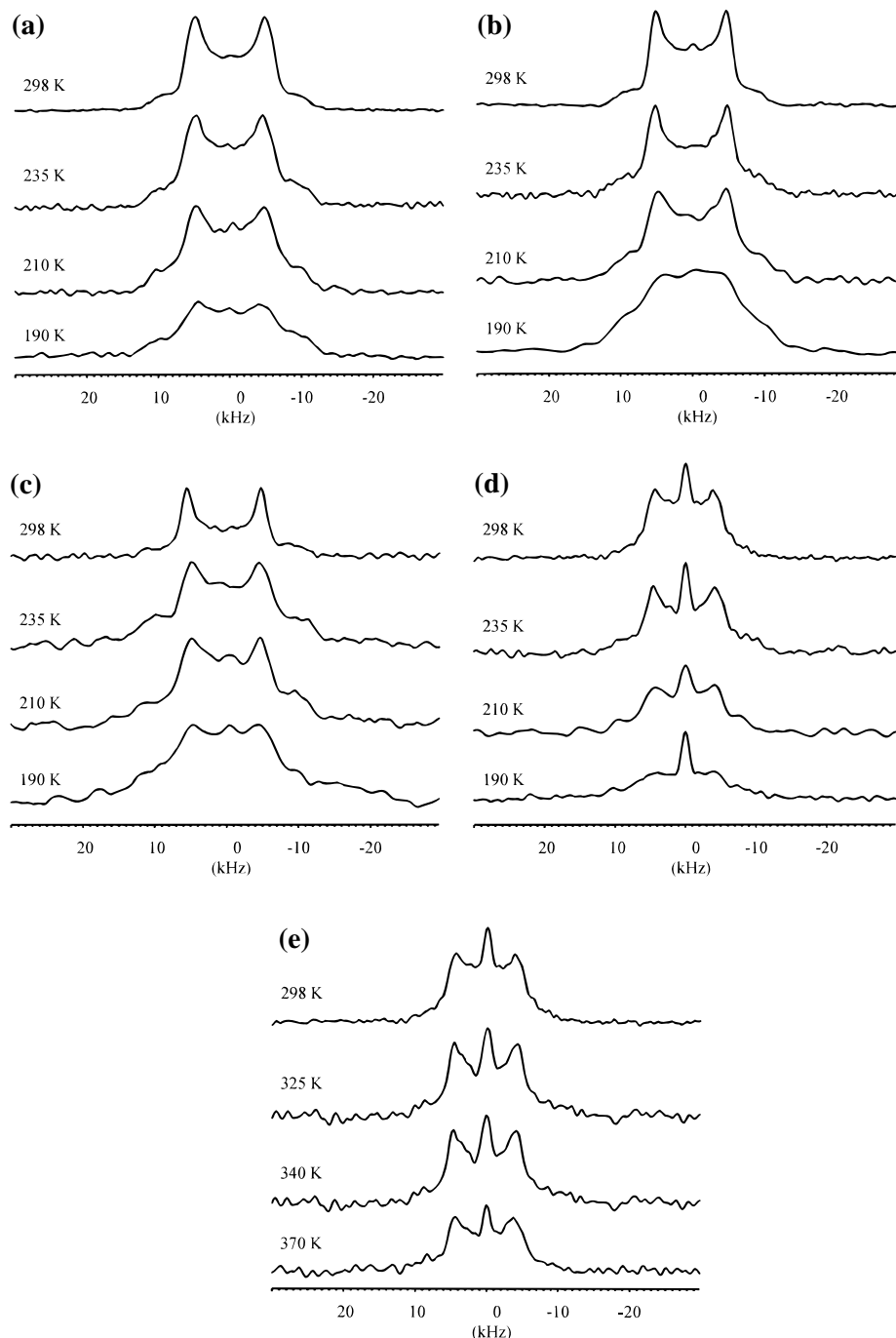


Figure 7. (a) Variable temperature ^2H NMR spectra for d_9 -TMC5 nonasil. (b) Variable temperature ^2H NMR spectra for d_9 -TMC6 nonasil. (c) Variable temperature ^2H NMR spectra for d_9 -TMC7 nonasil. (d) Low-temperature ^2H NMR spectra for d_9 -TMC3 nonasil. (e) High-temperature ^2H NMR spectra for d_9 -TMC3 nonasil.

deuterons about the C_3 axis of a methyl group) usually exhibit no asymmetry.²⁴ Asymmetry in the ^2H NMR line shape can arise from motions with a 2-fold symmetry axis, such as flipping of a D_2O molecule about its C_2 axis.³⁴ We believe that the reduction in the observed QCCs and the presence of asymmetry in our samples are most likely due to an additional breathing motion of the methyl groups, a librational motion of the SDA, or both. The ^2H NMR results obtained do not let us distinguish between these possibilities. However, the two rotations account for about 95% of the observed reduction in the QCCs and they dominate the narrowing of the NMR spectra.

Variable Temperature ^2H NMR. Variable temperature ^2H NMR experiments were performed to study the strength of the organic–inorganic interactions. Variable temperature experi-

ments allow observation of the freezing out of motions at low temperatures, or the onset of liquidlike mobility at elevated temperatures. These changes in molecular mobilities will help to quantify the organic–inorganic interactions in the as-made nonasil samples. Molecular dynamics simulations predict that steric effects alone should prevent the TMC5, TMC6, and TMC7 structure-directing agents from isotropic rotation. For the TMC3 structure-directing agent, however, the nonasil cage does not exhibit sufficient steric confinement to prevent isotropic rotation.

The variable temperature ^2H NMR spectra of d_9 -TMC5 nonasil are shown in Figure 7a. The line shape has lost the sharp features of the Pake doublet at 190 K. The results at this temperature suggest the rotation rates are reaching the intermediate motion regime,³⁴ where the rate of the motion is the

same order of magnitude as the NMR time scale. Most likely the rotation about the R–N bond is the slower motion, consistent with work done by Vega⁴¹ on *d*₉-trimethylamine (this will be further addressed using *T*₁ experiments, vide infra).

The variable temperature ²H NMR spectra for *d*₉-TMC6 nonasil are shown in Figure 7b. The spectrum at 190 K also shows a loss of the Pake doublet similar to the *d*₉-TMC5 nonasil sample.

Variable temperature ²H NMR spectra for the *d*₉-TMC7 nonasil sample are shown in Figure 7c. The shoulders of the doublet are substantially broader at 190 K than any of the other samples, possibly indicating that the rotation about the nitrogen C₃ axis is slower in this sample. This is the largest structure-directing agent and the most sterically confined.

The trends observed in the variable temperature ²H NMR spectra for the TMC5, TMC6, and TMC7 nonasil systems follow the relative sizes of the molecules and are similar to the results for the neat solid salts. In all three samples two major rotations are observed, the rotation along the nitrogen C₃ axis and along the methyl group C₃ axes. The rotation along the nitrogen C₃ axis appears to slow to the order of the NMR time scale at 190 K. The rotation rates will be quantified using ²H *T*₁ experiments described below. Variable temperature ²H NMR was also performed on the *d*₉-TMC5, -TMC6, and -TMC7 nonasil samples between 298 and 370 K (not shown). For all samples the spectra did not change appreciably between 298–370 K.

The variable temperature results for the *d*₉-TMC3 nonasil sample are shown in Figure 7d,e. Simulations of the 298 K spectrum for this sample gives a smaller QCC of 13.5 kHz and a larger asymmetry of $\eta = 0.14$ than for the other three nonasil samples. The differences suggest that in this case there is an additional motion that introduces significant asymmetry into the line shape of the ²H NMR spectrum, likely librational in nature. The spectra for this sample also include a Lorentzian line which is approximately 8% of the total integrated intensity. The Lorentzian line is assigned to molecules undergoing isotropic reorientation on the NMR time scale, and the peak intensity is invariant to temperature within the temperature range investigated (see Figure 7d,e). One plausible explanation for the presence of the Lorentzian line is a small fraction of the [5⁸6¹²] cages containing two organic molecules which rotate isotropically between two sites in the cage. Energy minimization calculations show that the TMC3 structure-directing agent is small enough for the [5⁸6¹²] cage to accommodate two TMC3 molecules. Another possibility is that a fraction of the cages contain both a structure-directing agent and a sodium ion. The elemental analysis results indicate that 90% of the cages contain structure-directing agents, and nearly 20% of the cages in the TMC3–NON sample contain sodium (on a weight basis). At this point the available data do not allow us to distinguish between the two alternatives.

The main point is that at all temperatures up to 370 K more than 90% of the structure-directing agents are *not* isotropically reorienting. The TMC3 structure-directing agent is small and is *not* sterically prevented from isotropic reorientation; as a result we can conclude there are forces between the structure-directing agent and the framework that restrict the mobility of the TMC3 molecule. The lack of rapid reorientation in the TMC3–NON sample is in sharp contrast to nonasil samples made with electrically neutral amines. Gies¹⁷ has shown that the 2-aminopentane used to synthesize nonasil reorients isotropically in the 5⁸6¹² cage. The difference in mobilities observed suggest that the forces between the structure-directing agent and the nonasil framework are electrostatic in nature.

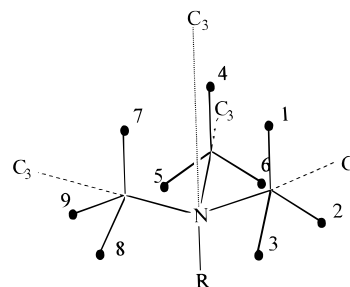


Figure 8. Model used for ²H NMR line shape simulations.

TABLE 5: Variable Temperature Spin–Lattice Relaxation Times (*T*₁) and Jumping Frequencies *k*₁ and *k*₂ for *d*₉-TMC6 Nonasil Using the 9-site Jump Model

temperature (K)	<i>T</i> ₁ ms	<i>k</i> ₁ (s ⁻¹)	<i>k</i> ₂ (s ⁻¹)
240	5.7	7.8×10^8	9.0×10^7
298	21.7	7.0×10^9	5.8×10^8
340	28.2	8.3×10^9	7.0×10^8

²H NMR Relaxation Experiments. When molecular motions are fast on the NMR time scale, only a lower bound on the rate of motion can be estimated. Spin–lattice relaxation (*T*₁) experiments in conjunction with line shape simulations can be used to quantify the rates of rotations in the limit of fast motion.^{24–26} The spin–lattice relaxation time *T*₁ is a V-shaped function of the correlation time of the motion. The *T*₁ minimum is approximately 1 ms, and this corresponds to a correlation time (τ_{cMIN}) that is the inverse of the Larmor frequency (ω_L) of ²H (~46 MHz). Motions that are faster or slower than $\tau_{cMIN} \sim 1/\omega_L \sim 3 \times 10^{-9}$ s result in a longer *T*₁.

The line shapes are simulated with the program Fastpowder using two motions: the rotation along the nitrogen C₃ axis and the rotations of the methyl groups. The rate constant for the rotation along the nitrogen C₃ axis is *k*₂ and the rate constant for the rotation of the methyl groups is *k*₁. These rotations are simulated using a nine site jump modeled as shown in Figure 8 and for simplicity, the two rotations were not coupled (i.e., jumps from site 1 to sites 2, 3, 4, and 7 are allowed, but jumps from site 1 to site 5 are not). The bending motion discussed above was not accounted for in the simulation, because the two rotations capture the essential features of the NMR line shape and the molecular motion. The motion of the structure-directing agent is a composite motion, as a result, the line shape simulations can be done with nonunique values of the rate constants for the different motions. Work by Vega⁴¹ on solid *d*₉-trimethylamine indicates that the rotation along the nitrogen C₃ axis is the slower of the motions and this constraint is used in the line shape simulations.

Variable temperature *T*₁ experiments were performed on the *d*₉-TMC6 nonasil sample to verify that the rotation about the nitrogen C₃ axis is the slower of the two motions (Table 5). On the basis of the known temperature dependence of *T*₁ we can predict how *T*₁ should change with temperature (motion rate). Specifically, the rate of motion should increase as the temperature increases, resulting in a longer *T*₁ if the motion rate constants at 298 K are larger than $1/\tau_{cMIN}$. The variable temperature results are listed in Table 5, and *T*₁ decreases as the temperature decreases between 240–340 K. At the lowest temperature of 240 K the simulated *k*₂ is less than τ_{cMIN} , which means the motion rate likely crossed the minima of the *T*₁ curve between 298 and 240 K. Nevertheless, these results show that the rotation rates are faster than $1/\tau_{cMIN}$ at 298 K.

Room-temperature *T*₁ experiments were performed on the four samples and are summarized in Table 4. The values of the

spin–lattice (T_1) relaxation time are consistent with size effects. On the basis of the variable temperature T_1 results for the d_9 -TMC6 sample, we can conclude that for all samples the methyl group rotation rates are faster than $1/\tau_{\text{cMIN}}$ at 298 K. The rate constants used for the 298 K line shape simulations (not shown) also verify that the rotation about the R–N bond axis is slowest in the d_9 -TMC7 sample.

^2H MAS NMR. One of the major limitations of static ^2H NMR experiments is the need for relatively high concentrations of ^2H in the sample. For our samples with deuterium labeled alkyl groups, there is approximately 0.07 wt % deuterium in the sample. The combination of a small amount of deuterium present in the sample, the small amount of sample used (~ 50 mg in the static probe), and the low receptivity of ^2H (about 100 times weaker than ^{13}C) results in very long acquisition times. Single-pulse MAS³⁵ experiments can be used to improve the signal-to-noise ratio. The signal-to-noise ratio improves because of an increase in sample volume (4 mm MAS rotors) and because all the spectral information is contained in sharp spinning sidebands. The MAS experiments can also be used effectively with soft pulses compared to the traditional static experiments. For these reasons we have used ^2H MAS NMR rather than the traditional static quadrupole echo experiment to study the dynamics of structure-directing agents with deuterium-labeled substituent alkyl groups. This experimental technique is limited in our case because spectrometer CPU memory constraints limit the size of the FID. This makes phasing the spectra problematic, and as a result the ^2H MAS results presented here are only qualitative.

As a comparison to the static experiments, Figure 9a shows the static and MAS spectra for the d_9 -TMC5 nonasil sample (spin rate $\nu_r = 2.00$ kHz). The envelope of the spinning sidebands of the MAS spectrum is in good qualitative agreement with the results from the static experiments. Figure 9b contains the ^2H MAS spectrum of the d_1 -TMC5 nonasil sample spun at 6.0 kHz. The theoretical QCC value for a rapidly puckering but otherwise immobile cyclopentyl ring is approximately 110 kHz.⁴³ The line shape at 298 K has a QCC of approximately 95 kHz. This QCC value is consistent with a rapid puckering of the cyclopentyl ring, with some additional librational motion. The additional reduction in the QCC from 110 kHz could also be due to small angle rotations about the R–N axis. Free rotation of the cyclopentyl ring can be ruled out as this motion would result in a QCC at least a factor of 2 smaller than the observed value. Molecular dynamics simulations predict that the cyclopentyl ring will undergo small angle rotations about the R–N bond on the nanosecond time scale. The small angle rotations would lead to a reduction in the QCC from the value of 110 kHz for a nonrotating, rapidly puckering cyclopentyl ring.

Figure 9c shows the ^2H MAS spectrum for the d_1 -TMC7 nonasil sample spun at 6.0 kHz. Simulating this spectrum results in a QCC of 110 kHz. The QCC value can be attributed to a fixed norbornyl ring with librational motion. The static ^2H NMR spectrum for the d_1 -TMC7 structure-directing agent indicates the ring is fixed (not shown). The synthesis by Brown et al.³¹ to make the ring deuterated amine yields the exo-isomer of norbornylamine. In our sample, however, the deuterium may be cis-, trans-, or a mixture of both to the trimethylammonium group. For those reasons, the ^2H MAS spectrum may be the superposition of more than one signal. Nonasil can be made with both the endo- and exo-forms of norbornylamine,¹³ but this may lead to a distribution of mobilities. Due to equipment limitations, phasing the MAS spectra was problematic and a

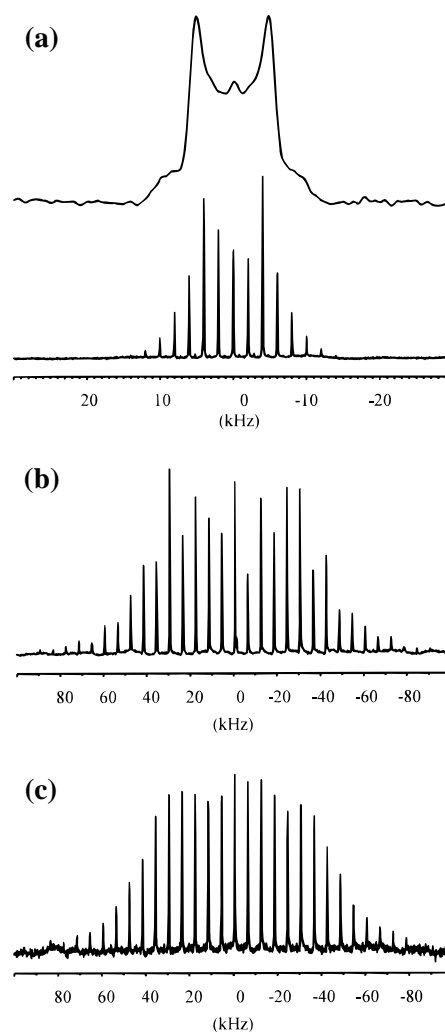


Figure 9. (a) Comparison of static ^2H and ^2H MAS NMR spectra of d_9 -TMC5 nonasil. Spin rate $\nu_r = 2.0$ kHz for MAS spectrum. ^2H MAS NMR spectra of (b) d_1 -TMC5 nonasil, and (c) d_1 -TMC7 nonasil. Spin rate $\nu_r = 6.0$ kHz.

quantitative analysis of the line shapes is not possible. The lack of mobility of the rings are, however, reflected in the values of the QCCs obtained.

Summary

The dynamics of several organic structure-directing agents in the as-made zeolite nonasil have been characterized using ^2H NMR spectroscopy. All structure-directing agents with deuterated methyl groups show fast methyl group internal rotations and rotation about the nitrogen C_3 axis down to 190 K. Three of the four structure-directing agents are sterically prevented from isotropic reorientation, but the smallest one, TMC3, is not. Nevertheless, approximately 90% of the structure-directing agents in the TMC3–NON sample are not isotropically reorienting at 370 K. The results clearly show strong electrostatic interactions between the organic molecules and the zeolite framework. This in contrast to nonasil samples made with electrically neutral amines, where van der Waal forces dominate. The steric factors imposed on the structure-directing agents by the nonasil structure are clearly illustrated by the ^2H NMR T_1 experiments as well as by the ^2H MAS NMR spectra of samples with deuterated substituent alkyl groups.

The defect sites have been characterized using ^{29}Si and ^1H NMR. The ^{29}Si results indicate the as-made materials contain

approximately four Q³ per cage. The ¹H NMR results indicate that the silanol groups participate in hydrogen bonding with the siloxy groups, consistent with the work of Koller et al.³⁷ On the basis of these results we can conclude that the defect sites are in close proximity either as isolated pairs or larger clusters. One unanswered question is whether the orientation of the trimethylammonium group is correlated toward the defect site. We are pursuing this issue using two-dimensional ²⁹Si–¹H correlation NMR spectroscopy.

Though nonasil is a model system, these results should hold qualitatively for other all-silica materials. The lack of mobility of the TMC3 molecule can only be attributed to electrostatic interactions, which should be present in any all-silica zeolite made with a cationic structure-directing agent. Extrapolation to synthesis conditions must be done with some hesitation, but there are clearly forces between the nonasil framework and the structure-directing agent that cannot be overcome by the thermal energy available at 370 K. These interactions could also be present at synthesis conditions (433 K). Systems where a small amount of boron or aluminum are used in the synthesis are more complex. In addition to the cationic structure-directing agents used, extraframework cations compete to balance the charge of the aluminum/boron.⁴⁴ If these organic–inorganic interactions are stronger than inorganic (Al/B)–inorganic (Na, K, etc.) interactions it may lead to selective incorporation of the aluminum/boron in the framework in close proximity to the charge on the structure-directing agent during the synthesis. This would have important implications about the possibility of tailoring the distribution of catalytically active sites in zeolites.

Acknowledgment. We are grateful to the regents of the ACS-PRF fund for financial support. The authors thank the Department of Chemistry and Biochemistry at the University of Delaware for use of the NMR spectrometer, C. Dybowski for useful discussions about the NMR results, and R. Griffin for use of the deuterium NMR line shape simulation programs. The authors also thank S. Zones (Chevron) for help with the nonasil synthesis and elemental analysis on the samples and E. Gaffney and M. Feuerstein for help with the solid-state NMR spectrometer.

Supporting Information Available: ¹³C liquid NMR spectrum of *N,N,N*-trimethylnorbornylammonium iodide with and without deuterium β to the trimethylammonium group, ¹³C CP-MAS NMR spectrum of TMC3–NON, SEM micrographs of TMC5–NON and TMC3–NON, ²H NMR spectra of the neat structure-directing agents, ²H NMR line shape simulations with and without additional breathing motion, and the ²H NMR *T*₁ results and simulations for the *d*₉-TMC6 nonasil sample at 298 and 340 K (14 pages). Ordering information is given on any current masthead page.

References and Notes

- (1) (a) Darby, N. *J. Protein Structure*; Oxford: New York, 1993. (b) Everett, D. H. *Basic Principles of Colloidal Science*; Royal Society of Chemistry: London, 1988. (c) Philp, D.; Stoddart, J. F. *Angew. Chem., Int. Ed. Engl.* **1996**, *35*, 1155.
- (2) VanSanten, R. A.; Kramer, G. J. *Chem. Rev.* **1995**, *15*, 637.
- (3) (a) Barrer, R. M. *Hydrothermal Chemistry of Zeolites*; Academic Press: London, 1982. (b) Moscou, L. *Stud. Surf. Sci. Catal.* **1989**, *58*, 1. (c) Breck, D. W. *Zeolite Molecular Sieves*; Wiley: New York, 1974.
- (4) (a) Wei, J. *Ind. Eng. Chem. Res.* **1994**, *33*, 246. (b) Klein, H.; Fuess, H.; Schrimpf, G. *J. Phys. Chem.* **1996**, *100*, 11101. (c) Snurr, R. Q.; Bell, A. T.; Theodorou, D. N. *J. Phys. Chem.* **1994**, *98*, 11948.
- (5) (a) Kubota, Y.; Helmkamp, M. M.; Zones, S. I.; Davis, M. E. *Microporous Mater.* **1993**, *6*, 213. (b) Hong, S. B.; Cambor, M. A.; Davis, M. E. *J. Am. Chem. Soc.* **1997**, *119*, 76. (c) Hong, S. B.; Cho, H. C.; Davis, M. E. *J. Phys. Chem.* **1993**, *97*, 1622.
- (6) (a) Burkett, S. L.; Davis, M. E. *J. Phys. Chem.* **1994**, *98*, 4647. (b) Zones, S. I. *Zeolites* **1989**, *9*, 458. (c) Gies, H.; Marler, B. *Zeolites* **1992**, *12*, 42. (d) Lobo, R. F.; Zones, S. I.; Davis, M. E. *J. Inclusion Phenom. Mol. Recognit. Chem.* **1995**, *21*, 47. (e) Zones, S. I.; Nakagawa, Y.; Yuen, L. T.; Harris, T. V. *J. Am. Chem. Soc.* **1996**, *118*, 7558. (f) Burkett, S. L.; Davis, M. E. *Chem. Mater.* **1995**, *7*, 1453.
- (7) Flanigen, E. M.; Bennet, J. M.; Grose, R. W.; Cohen, J. P.; Patton, R. L.; Kirchner, R. M.; Smith, J. V. *Nature (London)* **1978**, *271*, 512.
- (8) Lawton, S. L.; Rohrbaugh, W. J. *Science* **1990**, *247*, 1319.
- (9) Lobo, R. F.; Pan, M.; Chan, I. Y.; Li, H. X.; Medrud, R. C.; Zones, S. I.; Crozier, P.; Davis, M. E. *Science* **1993**, *262*, 1563.
- (10) (a) Gies, H.; Marler, B.; Fyfe, C. A.; Kokotailo, G.; Feng, Y.; Cox, D. E. *J. Phys. Chem. Solids* **1991**, *52*, 1235. (b) Lobo, R. F.; Pan, M.; Chan, I.; Medrud, R. C.; Zones, S. I.; Crozier, P. A.; Davis, M. E. *J. Phys. Chem.* **1994**, *98*, 12040. (c) Knops-Gerrits, P. P.; De Vos, D. E.; Peijnen, E. J. P.; Jacobs, P. A. *Microporous Mater.* **1997**, *8*, 3. (d) Engelhardt, G.; Michel, D. *High-Resolution Solid State NMR of Silicates and Zeolites*; Wiley: Chichester, 1987. (e) Davidson, A.; Weigel, S. J.; Bull, L. M.; Cheetham, A. K. *J. Phys. Chem. B* **1997**, *101*, 3065. (f) Pan, M. *Micron* **1996**, *27*, 319. (g) Terasaki, O.; Oshuna, T.; Ohnishi, N.; Hiraga, K. *Curr. Opin. Solid State Mater. Sci.* **1997**, *2*, 14. (h) Thomas, J. M.; Vaughan, D. E. W. *J. Phys. Chem. Solids* **1989**, *50*, 449.
- (11) Marler, B.; Dehnhostel, N.; Eulert, H. H.; Gies, H.; Liebau, F. J. *Inclusion Phenom.* **1986**, *4*, 339.
- (12) Marler, B.; Gies, H. *Zeolites* **1995**, *15*, 517.
- (13) Harris, T. V.; Zones, S. I. *Stud. Surf. Sci. Catal.* **1994**, *64*, 29.
- (14) Balkus, K. J. Jr.; Shepelev, S. *Microporous Mater.* **1993**, *1*, 383.
- (15) Behrens, P.; van de Goor, G.; Freyhardt, C. C. *Angew. Chem., Int. Ed. Engl.* **1995**, *34*, 2680.
- (16) van de Goor, G.; Freyhardt, C. C.; Behrens, P. Z. *Anorg. Allg. Chem.* **1995**, *621*, 311.
- (17) Gies, H. In *Inclusion Compounds*; Atwood, J. L., Davies, J. E. D., MacNicol D. D., Eds.; Oxford: New York, 1991; Vol. 5 (Inorganic and Physical Aspects of Inclusion).
- (18) Fyfe, C. A.; Mueller, K. T.; Kokotailo, G. T. In *NMR Techniques in Catalysis*; Bell, A. T., Pines, A. Eds.; Marcel Dekker: New York, 1994.
- (19) Rohr-Schmidt, K.; Spiess, H. W. *Multidimensional Solid-State NMR and Polymers*; Academic: London, 1994.
- (20) (a) Klinowski, J.; Carpenter, T. A.; Thomas, J. M. *J. Chem. Soc., Chem. Commun.* **1986**, 956. (b) Barron, P. F.; Frost, R. L.; Skjemstad, J. O. *J. Chem. Soc., Chem. Commun.* **1983**, 581. (c) Fyfe, C. A.; Wong-Moon, K. C.; Huang, Y.; Grondey, H.; Mueller, K. T. *J. Phys. Chem.* **1995**, *99*, 8707. (d) Engelhardt, G.; Lohse, U.; Samoson, A.; Magi, M.; Tarmak, M.; Lippma, E. *Zeolites* **1982**, *2*, 59. (e) Fyfe, C. A.; Grondey, H.; Feng, Y.; Kokotailo, G. T.; Ernst, S.; Weitkamp, J. *Zeolites* **1992**, *12*, 50.
- (21) (a) Hunger, M.; Engelhardt, G.; Koller, H.; Weitkamp, J. *Solid State Nucl. Magn. Reson.* **1993**, *2*, 111. (b) Feuerstein, M.; Hunger, M.; Englehardt, G.; Amoureux, J. P. *Solid State Nucl. Magn. Reson.* **1996**, *7*, 95. (c) Koller, H.; Burger, B.; Schneider, A. M.; Engelhardt, G.; Weitkamp, J. *Microporous Mater.* **1995**, *5*, 219.
- (22) (a) Vega, A. J.; Luz, Z. *J. Phys. Chem.* **1986**, *90*, 4103. (b) Kustanovich, I.; Luz, Z.; Vega, S.; Vega, A. J. *J. Phys. Chem.* **1990**, *94*, 3138. (c) Eckman, R. A.; Vega, A. J. *J. Phys. Chem.* **1986**, *90*, 4679. (d) Silbernagel, B. G.; Garcia, A. R.; Newsam, J. M.; Hulme, R. J. *J. Phys. Chem.* **1989**, *93*, 6506. (e) Vega, A. J.; Luz, Z. *Zeolites* **1988**, *8*, 19.
- (23) Vold, R. R. In *Nuclear Magnetic Resonance Probes of Molecular Dynamics, Understanding Chemical Reactivity*; Tycko, R., Ed.; Kluwer: London, 1994; Vol. 8.
- (24) Torchia, D. A.; Szabo, A. J. *Magn. Reson.* **1982**, *49*, 107.
- (25) Vold, R. R.; Vold, R. L. In *Advances in Magnetic and Optical Resonance*; Warren, W. S., Ed.; Academic: San Diego, 1991; Vol. 16.
- (26) Wittebort, R. J.; Olejniczak, E. T.; Griffin, R. G. *J. Chem. Phys.* **1987**, *86*, 5411.
- (27) (a) Bull, L. M.; Henson, N. J.; Cheetham, A. K.; Newsam, J. M.; Heyes, S. J. *J. Phys. Chem.* **1993**, *97*, 11776. (b) Hepp, M. A.; Ramamurthy, V.; Corbin, D. R.; Dybowski, C. R. *J. Phys. Chem.* **1992**, *96*, 2629. (c) Auerbach, S. M.; Bull, L. M.; Henson, N. J.; Metiu, H. I.; Cheetham, A. K. *J. Phys. Chem.* **1993**, *100*, 5923.
- (28) (a) Sidhu, P. S.; Bell, J.; Penner, G. H.; Jeffrey, K. R. *Can. J. Chem.* **1995**, *73*, 2196. (b) Meirovitch, E.; Belsky, I.; Vega, S. J. *J. Phys. Chem.* **1984**, *88*, 1522. (c) Ripmeester, J. A.; Ratcliffe, C. I. In *Inclusion Compounds*; Oxford: New York, 1991; Vol. 5 (Inorganic and Physical Aspects of Inclusion). (d) Meirovitch, E.; Belsky, I. *J. Phys. Chem.* **1984**, *88*, 4308. (e) Collins, M. J.; Ratcliffe, C. I.; Ripmeester, J. *J. Phys. Chem.* **1990**, *94*, 157.
- (29) den Ouden, C. J. J.; Datema, K. P.; Visser, F.; Mackay, M.; Post, M. F. M. *Zeolites* **1991**, *11*, 418.
- (30) All-silica material: No trivalent cations (B, Al, etc.) have been purposely added to the synthesis mixture.
- (31) Brown, H. C.; Kim, K. W.; Srebnik, M.; Singaram, B. *Tetrahedron* **1987**, *41*, 4071.

(32) Langford, I. J. Lapod; School of Physics and Space Research: University of Birmingham, B15 2TT U.K.

(33) Powles, J. G.; Strange, J. H. *Proc. Phys. Soc.* **1963**, 82, 6.

(34) Spiess, H. W.; Sillescu, H. *J. Magn. Reson.* **1981**, 42, 381.

(35) Kristensen, J. H.; Bildsøe, H.; Jakobsen, H. J.; Nielsen, N. C. *J. Magn. Reson.* **1991**, 92, 443.

(36) In general, the chemical analyses overestimate the C/N ratio by approximately 20%. We believe that this difference is due to the difficulty of releasing the structure-directing agent occluded in the cages of nonasil. ¹³C CP-MAS NMR unambiguously confirms that the structure-directing agents are intact inside the nonasil cages.

(37) Koller, H.; Lobo, R. F.; Burkett, S. L.; Davis, M. E. *J. Phys. Chem.* **1995**, 99, 12588.

(38) (a) Nagy, J. B.; Gabelica, Z.; Derouane, E. G. *Chem. Lett.* **1982**, 1105. (b) Dessau, R. M.; Smith, K. D.; Kerr, G. T.; Woolery, G. L.;

Aleman, L. B. *J. Catal.* **1984**, 104, 484. (c) Woolery, G. L.; Aleman, L. B.; Dessau, R. M.; Chester, A. W. *Zeolites* **1986**, 6, 14.

(39) (a) Hunger, M.; Karger, J.; Pfeifer, H.; Caro, J.; Zibrowius, B.; Bulow, M.; Mostowicz, R. *J. Chem. Soc., Faraday Trans. 1* **1987**, 83, 3459.

(b) Chezeau, J. M.; Delmotte, L.; Guth, J. L.; Soulard, M. *Zeolites* **1989**, 9, 78. (c) Moser, W. R.; Thompson, R. W.; Chiang, C. C.; Tong, H. *J. Catal.* **1989**, 117, 19.

(40) Eckert, H.; Yesinowski, J. P.; Silver, L. A.; Stolper, E. M. *J. Phys. Chem.* **1988**, 92, 2055.

(41) Luz, Z.; Vega, A. *J. Chem. Phys.* **1987**, 86, 1803.

(42) Maus, D. C.; Copie, V.; Sun, B.; Griffiths, J. M.; Griffin, R. G.; Luo, S. Schrock, R. R.; Liu, A. H.; Seidel, S. W.; Davis, W. M.; Grohmann, A. *J. Am. Chem. Soc.* **1996**, 118, 5665.

(43) Meirovitch, E. *J. Phys. Chem.* **1984**, 88, 6411.

(44) Zones, S. I.; Van Nordstrand, R. A. *Zeolites* **1988**, 8, 16.